Plausibility Assessment of Numerical Cyclist to Vehicle Collision Simulations based on Accident Data

Niclas Trube, Patrick Matt, Marcin Jenerowicz, Niranjan Ballal, Thomas Soot, Dirk Fressmann, Nikolay Lazarov, Joerg Moennich, Thomas Lich, Patrick Lerge, Lennart V. Nölle, Syn Schmitt

Abstract According to recent traffic accidents statistics, the number of bicycle accidents has not been decreasing since 2010 and is even increasing in Germany. In the past, human body models were used to gain further insight into the kinematics and injury prediction for pedestrians and were validated for vehicle collisions based on post mortem human subject test data. As comparable validation data is not available for cyclists, data from accident databases offers the opportunity to compare simulation results with reality. In this study, three accidents were selected where the dimensions of the involved cyclist and vehicle matched those of the selected human body model (THUMS) and of the car model (Toyota Camry). The boundary conditions of the collision simulation were defined according to the GIDAS documentation. Data from the simulation on collision points, injury-inducing contact pairs and injury predictions were compared with GIDAS. The results of the simulations mostly matched the documented collision data very well. The data suggests that finite element simulation using state-of-the-art human body models can be used to reconstruct accident data, thus increasing trust in the simulation of collision scenarios, where a validation is currently not possible.

Keywords accident reconstruction, cyclist to vehicle collision, finite element analysis, human body model, plausibility assessment

I. INTRODUCTION

Recent traffic accident statistics show that the number of bicycle accidents has not been decreasing since 2010 in the EU [1] and is even increasing in Germany [2]. Another study found that 53 % of cyclist fatalities in the EU between 2015 and 2017 were caused by a collision with a passenger car [3]. Traffic accident statistics showed that roughly 80 % of all cyclists killed in accidents in the EU are male. This proportion remained almost constant between 2010 and 2019 [1, 3]. In the past, finite element (FE) simulations using human body models (HBMs) were used to further investigate the kinematics or injury risk of cyclists in vehicle collisions [4–6]. Some studies further compared the simulation results with data from real-life accidents [7–8]. However, little data is available on comparative studies of real-life accidents and FE-replications using HBMs, where both kinematics and whole-body injury assessment of the cyclist are investigated.

Several HBMs are available for occupant and pedestrian load cases [9–11], including the Total HUman Model for Safety (THUMS^{TM}) V4.02 AM50 Pedestrian [12], which was validated [13] based on experimental data from generic vehicle collisions with post mortem human subjects (PMHSs) [14–15]. To the best knowledge of the authors, experimental PMHS data from bicycle to generic vehicle collisions, which would enable a direct validation, is currently not available. The same is true for other types of vulnerable road users (VRUs), such as E-Scooter [16] or wheelchair users [17], except for pedestrians.

While the vehicle-to-VRU collision scenarios are quite similar for pedestrians and cyclists, they are not identical [18–19]. Real-life accident data, despite having more unknown or imperfect data available than experimental PMHS validation data, offers the opportunity to compare simulation results and injury predictions with reality for single, comparable VRU accident cases.

By comparing the simulation results with the accident data documentation, the *plausibility* of the FE

N. Trube (e-mail: niclas.trube@emi.fraunhofer.de, phone: +49 761 2714-394), P. Matt, M. Jenerowicz, N. Ballal and T. Soot are Research Fellows at Fraunhofer Institute for High-Speed Dynamics (EMI), Germany. D. Fressmann and N. Lazarov are Senior Engineers at DYNAmore GmbH, Germany. J. Moennich and T. Lich are Accident Research Specialists at Robert Bosch GmbH, Germany. P. Lerge and L.V. Nölle are Ph.D. researchers, S. Schmitt is Professor for Computational Biophysics and Biorobotics at the Institute for Modelling and Simulation of Biomechanical Systems of University of Stuttgart, Germany.

simulations can be checked, which is also referred to as *plausibility assessment* in this study. The term *plausibility* is used accordingly in the following sections regarding how well the extractable FE collision simulation data matches their available counterpart from the real-life accident data documentation for single collision cases.

As HBMs are an important tool to improve future traffic safety and are already part of the consumer information rating programme in Europe regarding kinematic evaluation for pedestrians [20], this study aims to gain further insights into the *plausibility* of cyclist collision simulation using HBMs to address the high risk of this VRU-type in traffic safety [3]. Data regarding collision points, injury-inducing contact pairs and injury assessment will be analysed and compared to their counterparts from the German In-Depth Accident Study (GIDAS) [21–22].

II. METHODS

This study is being conducted as part of the national research project *Artificial Intelligence for Real-Time Injury Prediction (ATTENTION)*. The *aim of ATTENTION* is to develop a method for real-time injury prediction of VRUs, such as pedestrians or cyclists as part of a proof-of-concept study. For this purpose, data-driven methods are used to determine a situation-specific injury risk from vehicle-based video data and virtual tests with the help of FE HBMs. Prospectively, the AI-based injury prediction shall enable both safe and efficient traffic through automated vehicle risk mitigation strategies.

Part of the project work involves the generation of large amounts of car-to-HBM collision simulations with different parameter combinations as training data for the AI-models. The parameter combinations comprise the relative velocities of the collision partners, the collision angle and the VRU position in front of the bumper. Further aspects of ATTENTION, as well as initial findings were previously published [18, 19, 23]. Within the scope of this study, a method will be presented by which individual simulations, as representatives of the training data points of ATTENTION, can be compared with real-life collision cases and checked for *plausibility*. Thus, this check for *plausibility* shall increase the trust in the generated training data based on individual data points within the parameter space. Based on the *aim of ATTENTION*, creating individual bicycle models, car models (including the verification of the windscreen) or individualised HBMs as a direct counterpart of the vehicles and VRUs involved in the single GIDAS cases is not intended and would exceed the scope of the project.

Considering this limitation, we developed a virtual setup for collisions, where the cyclist collides with the car front end. Each component (car, bicycle and cyclist) was compared to or developed based on data from the GIDAS database to allow for a comparison between the results from numerical cyclist to vehicle collision simulations and real-world collision data. Further details are provided in the following subsections.

Accident Case Selection

In this study, individual GIDAS cases were selected in which the dimensions of the front end were similar to the publicly available Toyota Camry vehicle model [24] and where the body size and weight match those of the validated Total HUman Model for Safety (THUMS^{TM}) V4.02 AM50 Pedestrian[1] [12]. The single GIDAS cases were further filtered regarding frontal vehicle-to-cyclist collision cases with large numbers of injuries. This is because one aim of this study is to compare the HBM-based injury prediction with the cyclist's sustained injuries documented in the GIDAS accident data. Due to the different injury risk levels that these selected probabilistic injury criteria can predict, which are described in further detail in the section *HBM Instrumentation and Injury Prediction* section and in the appendix (Table A-I to A-III), a direct comparison between injury prediction and sustained injuries is only possible if at least moderate injuries such as cortical bone fractures or traumatic brain injuries (TBI) were sustained and documented in GIDAS. Furthermore, these injuries must have been caused by the primary impact of the cyclist with the car or bicycle according to the GIDAS documentation.

Three of the resulting GIDAS cases[2], for which these criteria were met, were selected for FE accident reconstruction in this study. For these cases, the GIDAS injury information was compared with the probabilistic and deterministic injury prediction using THUMS in a frontal vehicle-to-cyclist collision simulation of the primary impact. In addition, minor injuries, such as contusions or abrasions, were discussed comparatively with the

[1] Throughout only the abbreviation "THUMS" will be used for the Total HUman Model for Safety (THUMS^{TM}) V4.02 AM50 Pedestrian used in this study.
[2] In this study, the GIDAS documentation of accident cases with the IDs 1050918, 1170986 and 30090880 were compared with simulation data.

available injury criteria of the corresponding body regions with the restriction that the injury criteria used were developed to predict a higher injury severity level.

In GIDAS, the assignment of injuries to contact points on the vehicle is done by the technical and medical investigation team by identifying the contact points (e.g. damage or wipe marks) on the vehicle while still at the scene of the accident. In addition, a data collection of the injuries is carried out on site or in hospital. The assignment of the individual injuries to the contact points on the vehicle is supported by the reconstruction team, which simulates the course of the accident.

TABLE I

COMPARISON OF THE FE CAR MODEL WITH THE GIDAS PASSENGER CARS

#GIDAS	#car	Mass [kg]	H1 [cm]	H2 [cm]	H3 [cm]	L1 [cm]	L2 [cm]	L3 [cm]
-	Camry	1603.8	77.1	99.9	136.2	12.2	111.4	185.0
1050918	car1	1530±[3]73.8	70.0±7.1	92.4±7.5	131.6±4.6	11.0±1.2	108.9±2.5	175.6±9.4
1170986	car2	1575±28.8	73.2±3.9	96.1±3.8	138.1±1.9	10.4±1.8	107.3±4.1	186.8±1.8
30090880	car3	1146±457.8	75.4±1.7	96.0±3.9	134.8±1.4	16.6±4.4	106.7±4.7	175.0±10

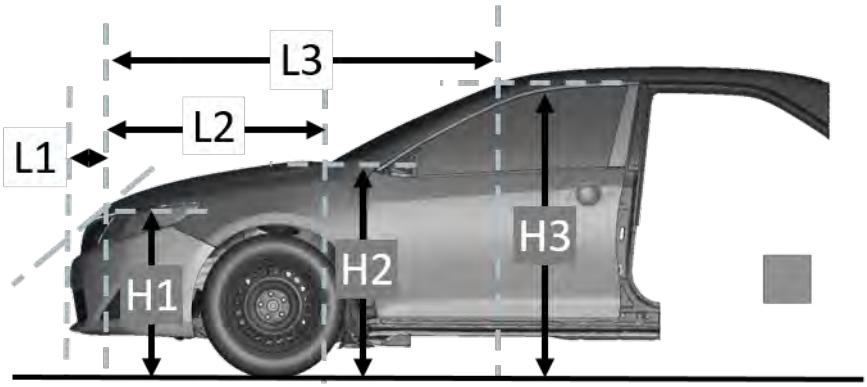

Fig. 1. Vehicle dimensions compared between the adapted FE model and the GIDAS cars in Table I. The FE model [24] was modified in terms of a load-case specific reduction and an adaption of the windshield.

TABLE II

COMPARISON OF THUMS TO THE GIDAS CYCLISTS

#GIDAS	Weight [kg]	Standing Height	Age
THUMS	77.2	178.2	-
1050918	75±2.2	177±1.2	32
1170986	80±2.8	180±1.8	33
30090880	81±3.8	174±4.2	56

Vehicle Selection and Modifications

Based on the original version [24], the Toyota Camry vehicle model was modified in two ways before usage in the collision simulation [23]:

1. Load-case specific reduction of the vehicle model complexity to reduce computational costs and storage space while retaining important kinematic and dynamic properties as well as computational stability (Fig. 1). For this, the mass of all parts that were not part of the front end was replaced by a cubical replacement mass;
2. Implementing a windshield model based on the latest results of the scientific community, consisting of a polyvinyl butyral (PVB) mid-layer and two outer glass layers, which was previously validated for VRU load cases. Further details on the comparison of experimental and numerical headform impactor to

[3] In contrast to the common usage of "±" symbol as the margin of error, the symbol was used in Table I and Table II to uniformly define a positive or negative divergence from the FE model dimensions.

windshield collisions, where VRU-safety relevant results are compared between experiment and simulation, are provided in the following. It should be mentioned that, considering the *aim of ATTENTION*, individual counterparts of the windshields used in the experiment were not modelled. Based on the available literature, representative load cases were selected and compared to the modified Toyota Camry windshield model used in this study, regarding the most important characteristics of the acceleration curve shape. Due to differences in the windshield geometries between experiment and simulation, certain deviations, such as for the peak values, are to be expected.

The PVB laminated windshield is widely recognised as an effective measure to reduce the severity of pedestrian injuries during vehicle-pedestrian collision scenarios. This type of windshield is modelled using different methods, for example, the single layer model consisting of a shell element sheet, and the three-layered model consisting of a PVB layer sandwiched between two glass layers [25]. The adapted windshield model in the present study features a three-layered construction that comprises a PVB layer sandwiched between two glass layers which is modelled using the latest results provided in literature [26–30].

The thickness of the glass layer and the PVB layer has been set to 2.1 mm and 0.76 mm, respectively, as suggested by [25]. In accordance with the research findings presented in literature [28–30], the PVB layer has been modelled as a hyper-elastic material, while the glass layer has been modelled as a glass material, as discussed by [28]. The assembly process employs shared nodes [31], which assume that the glass layer and the PVB layer are perfectly bonded with no relative displacements between them. Notably, the original assembly method of the windshield to the vehicle frame via spot-weld constraints used in the Toyota Camry model [24] does not allow for a realistic force transfer from the windshield to the frame during an impact. Therefore, in this study, the windshield is bonded to the vehicle frame using an adhesive layer of approximately 8 mm thickness applied along the contour of the windshield. The modelling technique and the material parameters for the adhesive layer are adapted from the National Highway Traffic Safety Administration (NHTSA) Accord vehicle model [32].

The use case of this study entailed the simulation of a vehicle-to-VRU collision, for which the windshield had been modified to suit the specific use case. To ensure the general applicability of this adapted windshield model for this specific use case, a series of numerical tests were conducted, utilising a standard EEVC headform impactor [26, 33]. These tests involved directing the headform impactor perpendicularly at the windshield at varying velocities and positions, in accordance with the boundary conditions outlined in [25, 27, 28]. The results of these simulations were then compared against real-world experiments conducted under identical boundary conditions by [25, 27, 28]. Due to different car models, geometrical parameters of the experimental and numerical windshields are not identical, which is why an exact replication of the experimental results cannot be expected based on the numerical analysis. However, general features can be compared.

During each test, the acceleration behaviour of the headform was analysed using a virtual accelerometer. The recorded acceleration data were then compared with the experimental result provided by [25, 27, 28], enabling a comprehensive comparison of the adapted windshield model. The comparison, as illustrated in Fig. 2 and A-Fig. 8, ensures that the behaviour of the test acceleration curves is generally very similar to the experimental curves. As explained in further detail in literature [28], there are three stages during the loading of the windshield. Initially a pre-fracture stage, followed by a fracture of the first and second glass layer, which correlates with the initial peaks in the acceleration curve. In the last stage, the PVB layer experiences large deformations, resulting in a rather flattened peak in the acceleration curve. The results confirm an acceptable predictive capability of the adapted windshield model considering the later use of the model in terms of the overall *aim of ATTENTION* and VRU-safety application with regard to the different geometries of the experimental and numerical windshields and the resulting expected deviation of, e.g., peak acceleration values.

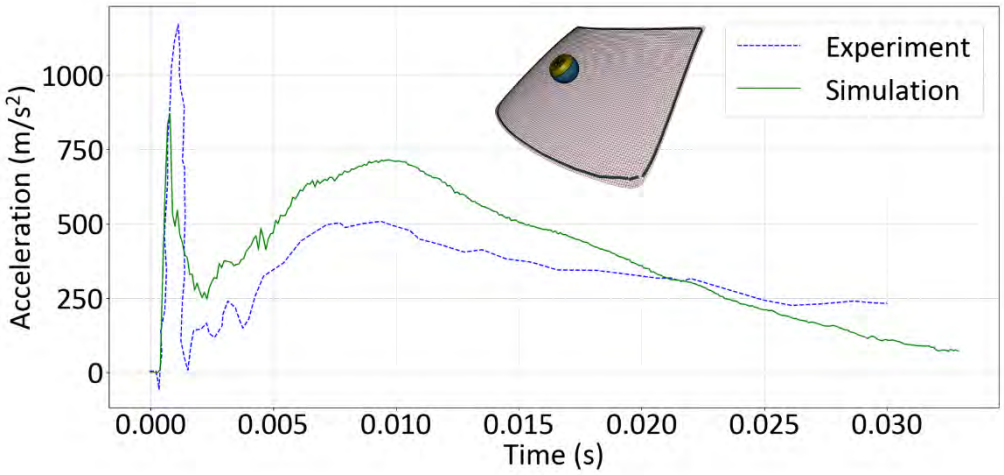

Fig. 2. Exemplary comparison of the acceleration behaviour of the headform with the experimental result of a standard EEVC headform impactor [33] impacting the windshield in the centre location [25, 27]. Further validation tests are provided in the Appendix.

HBM Positioning, Bicycle Model

The THUMS was positioned based on a mean cyclist-position extracted from vehicle-bound video documented car-cyclist collisions [18–19] and was slightly adapted to match the pedal positions, handlebar and saddle of the bicycle FE model. As the most common bicycle type from the analysed GIDAS data was a trekking bike, matching the results of other studies on GIDAS accident data [34], this bicycle type was selected for the modelling approach. The dimensions of the bicycle model (A-Fig. 4) are comparable to the European New Car Assessment Program (Euro NCAP) Cyclist AEB-Testing System (CATS) model [35]. In order to avoid deviations in the accident setup as best as possible, the dimensions of the bicycle were defined based on the median values of all bicycles involved in GIDAS accidents, where the involved car matched the dimensions of the Camry and the involved cyclist those of THUMS. Thus, this GIDAS bicycle might not have an identical counterpart in reality. In 81 % of the GIDAS cases, where the involved car matched the dimensions of the Camry and the involved cyclist those of THUMS, the cyclist did not wear a helmet. This includes the three cases selected for this study. Therefore, no helmet model was used for the FE accident reconstruction.

HBM Instrumentation and Injury Prediction

The THUMS was instrumented in order to obtain information regarding collision points and several injury criteria. Contact force transducer pairs were implemented to extract contact forces between VRU body regions and vehicle components for a measurable comparison of injury-relevant contact pairs between the accident data and the simulation, in addition to the subjective visual evaluation of collision points.

The following probabilistic injury criteria were considered for evaluation: Brain Injury Criterion (BrIC) [36], Cumulative Strain Damage Measure (CSDM) [36–38], Forman Rib Fracture Criterion [39, 40] (summarised in [41]), pelvis fracture criteria (deflection-based [42] and strain-based [43]), femur fracture criterion [44] and a tibia and fibula fracture criterion [44, 45]. The injury risk functions described in the respective sources, summarised in [13], were used in this study. For the strain-based pelvis fracture criterion [43], the 95th and 99th percentile values of the maximum principal strain (MPS) distribution (MPS95 and MPS99), which consider the maximum MPS values of each cortical pelvis element over time, are used as injury values. According to the previously mentioned sources, the *Abbreviated Injury Scale* (AIS) was used to define the injury risk from AIS1 (minor injury) to AIS5 (critical injuries) [46]. For the injury criteria CSDM and BrIC, the levels AIS1+ (AIS1 or higher) to AIS5+ (AIS5 or higher) were defined. For these criteria, the highest AIS level which exceeded a threshold of 50 % AIS-based injury risk was selected for the comparison with the respective accident data on sustained brain injuries. Further, deterministic injury prediction was considered for each cortical bone in THUMS separately, based on the MPS of all elements of the respective bone. MPS thresholds were obtained from the literature for pelvis cortical bones

(1.0 % MPS [47]) and all other cortical bones (1.5 % MPS [48–49]). Both probabilistic and deterministic whole-body injury predictions were used for comparison with the single GIDAS accident cases.

Collision Setup and Simulation Environment

By application of the explicit FE code MPP LS-DYNA R9.3 (LSTC), the numerical solution of each simulation was calculated using 32 cores on a Supermicro Computer (2.45 GHz AMD EPYC 7763 with 1024 GB RAM) running on Rocky Linux release 8.7. Based on the data collected from individual GIDAS accidents, a simulation matrix (Table III) was established for left-sided impacts, where the cyclist rode from the passenger side (right front end) to the driver side (left front end) of the vehicle. An averaged GIDAS deceleration of 3.5 m/s², defined based on data from previously filtered cases, for frontal collisions of passenger cars with cyclists and pedestrians, was applied to the front axis of the modified car model for all simulations. The collision angle and Y-Offset of each simulation are defined as shown in Table III. A reference image is shown in Fig. 3. The global coordinate system and the Y-Offset of the simulation setup are defined based on specifications in Euro NCAP TB024 [20]. For a Y-Offset of 0 mm, the centre of gravity of the THUMS head was aligned with the vehicle centreline.

TABLE III

PARAMETER DEFINITIONS OF COLLISION SIMULATION BASED ON GIDAS

#GIDAS	Car Velocity [km/h]	Cyclist velocity [km/h]	Y-Offset [mm]	Collision angle [°]
1050918	47	25	-750	226
1170986	30	12	-50	288
30090880	38	5	-100	274

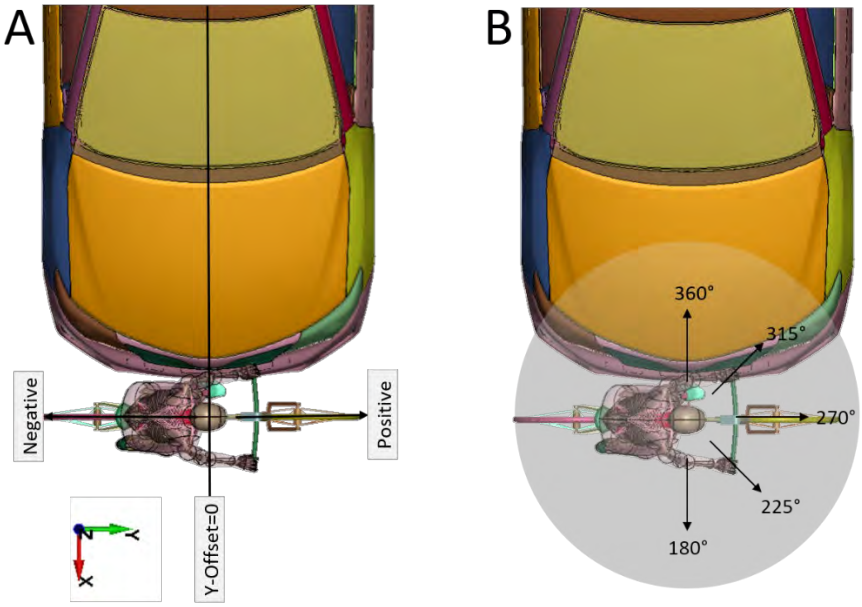

Fig. 3. Definition of the Y-Offset from the vehicle centreline (A) and of the collision angle (B).

III. RESULTS

The whole-body kinematics of case 1170986 are shown in Fig. 4 for the total simulation time of 400 ms with each image being 100 ms apart. The same information is provided for the other cases in the Appendix (A-Fig. 1 to A-Fig. 3).

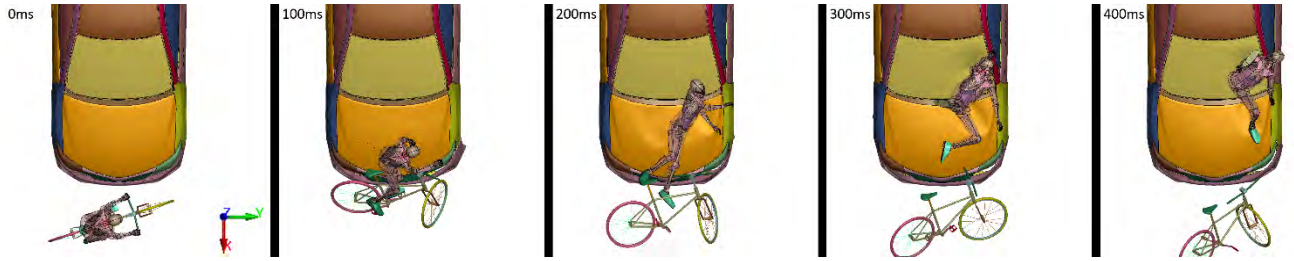

Fig. 4. Exemplary whole-body kinematics over time from simulation data for case 1170986.

The collision points between the cyclist and the vehicle model were visually evaluated for the FE simulation (Fig. 5). Collision points from the real-life collision were extracted from the GIDAS documentation, if available. Data was missing for GIDAS case 300090880 and was reconstructed based on dents in the bodywork, observable via photographs in the single case documentation.

#	GIDAS collision points	FE simulation
1170986	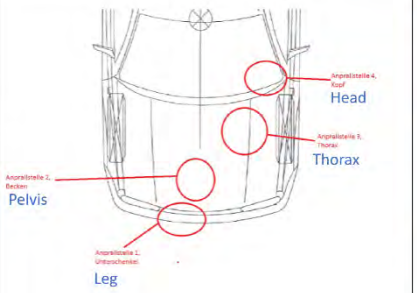	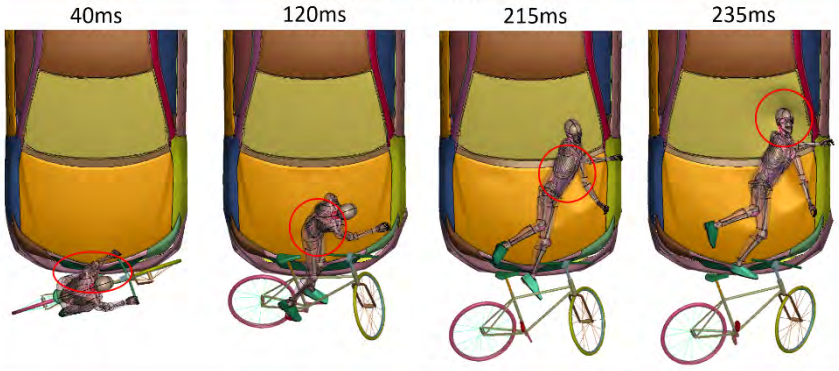

Fig. 5. Exemplary data on the collision points of the cyclist and the vehicle from the accident data and from the collision simulation regarding the documented body regions for case 1170986. English translations were added in blue based on the original image file from GIDAS.

#	GIDAS contact pairs and resultant contact forces
1170986	1) Bruise leg (left) → Bumper of opposing vehicle 2) Graze knee (left) → Hood of opposing vehicle 3) Graze D1 (left), inner ankle (left), leg (right) → Own bicycle, footpegs, pedals 4) Graze forehead (left), TBI l° → Windshield of opposing vehicle

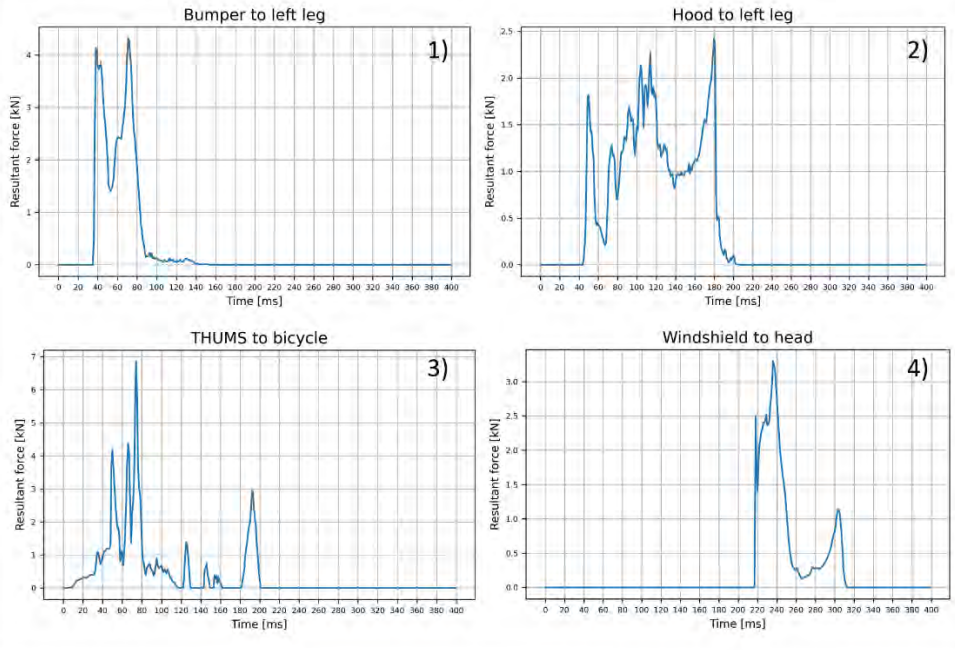

Fig. 6. Exemplary comparison of the injury-causing contact pairs in GIDAS with the contact force transducer data of the FE collision simulation for case 1170986.

By defining multiple contact pairs for different combinations of body regions and vehicle components, it was possible to compare injury-inducing contact pairs between GIDAS and the collision simulation (Fig. 6). For example in the 1170986 case, peaks in the contact force of the contact force transducer pairs *bumper to left leg* and *windshield to head* could be observed, where extremity injuries due to bumper contact and head injuries due to windshield contact were documented in the GIDAS file.

The results of injury predictions of the model using the deterministic method (DM) and probabilistic method (PM) are summarised in Table IV and are compared with the sustained injuries documented in the GIDAS cases. Further details are provided in the Appendix.

TABLE IV
COMPARISON OF INJURIES REPORTED IN GIDAS AND PREDICTED BY THE HUMAN BODY MODEL.

		1050918			1170986			30090880		
			HBM			HBM			HBM	
Body region		GIDAS	PM	DM	GIDAS	PM	DM	GIDAS	PM	DM
Head		TBI AIS2	AIS2+=72.9 % CSDM=0.35	-	TBI AIS2	AIS2+=57.8 % CSDM=0.28	-	TBI AIS2	AIS2+=80.2 % CSDM=0.39	-
Chest (rib fractures)		None	AIS1+=10.3 %	No	None	AIS1+=10.3 %	No	2	AIS1+=29.4 % AIS2+=2.46 %	Yes (1)
Pelvis		None	AIS2+=1.5 %	No	None	AIS2+=7.0 %	No	Bruise AIS1	AIS2+=37.9 %	Yes
Thigh	R	None	0.0 - 0.6 % (AIS3+)	Yes	None	0.0 % (AIS3+)	Yes	None	0.2 - 1.9 % (AIS3+)	Yes
	L	None	0.0 % (AIS3+)	No	None	0.0 - 0.6 % (AIS3+)	No	None	0.3 – 0.9 % (AIS3+)	None
Leg	R	None	0.1 - 1.3 % (AIS2+)	No	Graze (AIS1)	0.0 - 2.1 % (AIS2+)	No	None	0.6 - 2.6 % (AIS2+)	No
	L	Tibia, Fibula (AIS2)	1.5 – 10.5 % (AIS2+)	Yes	Bruise (AIS1)	1.2 – 9.4 (AIS2+)	Yes	None	1.1 – 36.2 % (AIS2+)	Yes

IV. DISCUSSION

In the following subsections, the results of each GIDAS simulation pair will be discussed separately, followed by a summary for all cases.

Case 1050918

Based on the data in Table I and Table II, the sizes of the VRU and vehicle match very well for case 1050918. A visual evaluation of the collision pairs (A-Fig. 5) shows a good agreement between the data of the simulation and the GIDAS case. The collision points of the leg and bumper as well as the head and the windshield are comparable between simulation and GIDAS. For the thorax, an impact on the windshield was documented in GIDAS, while a collision with the hood was observed in the simulation. This might partly be due to the slightly shorter front end length L3 compared to the FE model (Table I).

Data regarding contact forces (A-Fig. 6) obtained from contact force transducer pairs in the simulation matches the GIDAS documentation for both injury-inducing contact pairs (bumper to left leg and windshield to head). In detail, a local peak in contact force could be observed in the simulation for both contact pairs, with a maximum contact force of 3.5 kN for the bumper to left leg pair and 3.8 kN for the windshield to head pair.

The predicted injuries (Table IV) were in good agreement with the reported injuries from GIDAS. Head, chest, left thigh and tibia matched for GIDAS and the simulation. In the simulation, the tibia AIS2+ risk was rather low compared to the observed fracture in GIDAS. However, deterministic injury prediction clearly predicts a fracture based on MPS evaluation (Table A-I) for the tibia and near-fracture MPS for the fibula. However, the deterministic injury prediction, in contrast to the probabilistic injury prediction, does not consider the variance of sustained

injuries within populations for identical load cases. Therefore, the results from deterministic injury prediction need to be treated with caution, as i.e., individual differences in anatomy or response to loading are not considered.

Based on the results from deterministic injury prediction, a fracture of the right femur is predicted for all three GIDAS cases. As the reason for this behaviour can be related to the same origin for all three cases, this divergence from GIDAS will only be discussed for case 1050918 but is identically true for cases 1170986 and 30090880. The main reason for this difference is a divergence in the geometry of the crossbar of the GIDAS bicycles and the FE model (A-Fig. 4). In all GIDAS cases, the crossbar was either non-existent or located much lower than in the FE model. Thus, in GIDAS the right thigh was probably not in contact with the crossbar at all, which explains why no injuries (not even bruises) are documented for the thigh and femur. In the simulation, the vehicle collision results in a contact between the crossbar and the thigh. In return, this contact can lead to the exceeded MPS threshold for the right femur. This hypothesis is supported by data on the right patella, which was also in contact with the bicycle crossbar (Fig. 5). For the right patella, the threshold for deterministic fracture prediction was also exceeded (Table A-I), but no fracture was reported in GIDAS. For all three cases, the bicycle dimensions seem to have an influence on the injury outcome in the femur region. As the prediction of fractures only applies to the strain-based data of the right femur, which is only in contact with the bicycle (not with the vehicle), the results can be related to the contact between the bicycle crossbar and the thigh.

Case 1170986

Based on the data in Table I and Table II, the sizes of the VRUs and vehicles match very well for case 1170986. A visual evaluation of the collision pairs (Fig. 5, A-Fig. 5) shows a very good agreement between the data of the simulation and the GIDAS case. The collision points of the leg and bumper, pelvis and hood, chest and hood, as well as the head and the windshield are closely comparable. The small difference in the collision points of the hood and thorax, as well as the windshield and head might result from a slightly different standing height of the cyclist compared to the THUMS (Table II) and from small differences in the car geometry compared to the Camry model.

The data regarding contact forces (Fig. 6, A-Fig. 6) from simulation is in accordance with the GIDAS documentation for all injuries resulting from vehicle or bicycle contact. In detail, local peaks in contact force could be observed in the simulation for contact pairs corresponding to the injury-inducing contact pairs documented in GIDAS, with a maximum contact force of 4.3 kN for the bumper to left leg pair, 2.4 kN for the hood to left leg pair, 6.9 kN for the THUMS to bicycle pair and 3.3 kN for the windshield to head pair.

The predicted injuries (Table IV) were in good agreement with the reported injuries from GIDAS. Based on the comparison with the contact force of the bumper and the left leg (Fig. 6), as well as the injury risk in the left leg (Table A-II), there is a chance of there being a bruise in this collision scenario. However, the injury risk criteria used in this study were not developed or validated for the prediction of minor injuries, such as bruises or grazes. Therefore, a prediction of these minor injuries is not possible based on probabilistic or deterministic injury criteria. The deterministic injury predictions even suggest a fracture of the left tibia and fibula (Table IV and Table A-II). Regarding the differences in the right femur data between GIDAS and simulation, see the corresponding subsection of *Case 1050918*.

Case 30090880

Based on the data in Table I and Table II, the sizes of the VRUs and vehicles were in very good agreement with most of the values for case 30090880. The biggest difference regarding the vehicle mass and the VRU size in comparison to the FE model, compared to the other cases, can be seen for case 30090880.

A visual evaluation of the collision pairs (A-Fig. 5) shows a good match between the data of the simulation and the GIDAS case. A small shift to the vehicle passenger side can be observed in the simulation compared to GIDAS. The reason for this might be a different pedal position in GIDAS than in the simulation. Assuming that the left foot would be in the back pedal position instead of the front pedal position, the cyclist position during primary impact

(foot to bumper) would be shifted towards the vehicle driver side in order to match the primary collision points in the bumper region documented in GIDAS. Thus, all other contact points would also be shifted towards the driver side, resulting in a better match of the exact locations of the collision points between simulation and GIDAS. The exact pedal position is impossible to obtain from GIDAS accident reconstruction, as video data is not contained in the GIDAS documentation. FE simulations offer a good opportunity to predict details of collisions that would not be observable otherwise. Apart from this shift to the passenger side in the simulation, the contact pairs of the simulation correlated very well with GIDAS (left leg to bumper, pelvis to hood, as well as thorax and head to the windshield). Based on the *aim of ATTENTION* and due to time and resource constraints, a simulation of different pedal and foot positions was not possible in the context of this study. However, this would be an interesting aspect to investigate in future studies in this field.

Data regarding the contact forces (A-Fig. 6) from simulation matches the GIDAS documentation for all injuries resulting from vehicle or bicycle contact according to GIDAS. In detail, local peaks in contact force could be observed in the simulation for contact pairs corresponding to the injury-inducing contact pairs documented in GIDAS, with a maximum contact force of 0.5 kN for the hood to buttock pair, 1.0 kN for the hood to torso pair, 1.4 kN for the windshield to torso pair and 3.1 kN for the windshield to head pair.

The predicted injuries (Table IV) were in good agreement with the reported injuries from GIDAS. Based on the GIDAS documentation, the thorax collision might have occurred in the region of the windshield wipers (A-Fig. 5). However, the windshield wipers are not part of the FE car model. As the windshield wipers can be slightly stiffer than the surrounding windshield and hood, a collision of the thorax with the windshield wipers can lead to a peak punctual load placed on individual ribs. The lack of windshield wipers in the FE model might therefore be the reason for the underpredicted risk of rib fracture, despite the agreement of the thorax collision point (A-Fig. 5). In addition, a nasal bone fracture is reported in GIDAS, which suggests that the head or the entire upper body including the head was slightly rotated towards the vehicle during collision in GIDAS. Although the cyclist was slightly rotated towards the camry model in the simulation (Table III), the default position of the head or upper body was defined according to the mean cyclist posture previously obtained from video data analysis [19], which rather led to a windshield collision with the back of the head rather than the front of the head. A possible rotation of the upper body of the cyclist in GIDAS might also have led to the difference in the number of predicted fractured ribs in the simulation.

The 56-year-old cyclist sustained a bruise on the pelvis (AIS1). For the cortical bone of the pelvis, the MPS threshold of 1.0 % is exceeded with a maximum MPS of 1.2 %, thus overpredicting the sustained injury (Table A-III). The AIS2+ injury risk in the pelvis from the simulation ranged from 22.0 % (45-year-old) to 37.9 % (65-year-old) for MPS95, which on average matched the rather low AIS level from GIDAS, while the values of MPS99 overestimated the injury risk compared to this GIDAS case with AIS2+ greater than 88 %. For the left leg, the injury risk was increasing from the proximal to the distal end, with a maximum value of 36.2 % for the distal tibia region. Likewise, deterministic prediction suggests a tibia fracture, while there was no fracture documented in GIDAS. After consultation with GIDAS accident research specialists, an underrepresentation of less critical injuries, such as tibia bruises or fractures, can in general be assumed if more severe injuries, e.g., head or chest, are present. As there was much less documentation available on case 30090880 compared to the other cases, a lack of detailed information on this GIDAS accident can be assumed, resulting in possibly missing information on, e.g. tibia or fibula hairline fractures or full fractures. Regarding differences in the right femur data between GIDAS and simulation, see the corresponding subsection of *Case 1050918*.

General

For all GIDAS cases, collision simulation data matched the corresponding GIDAS documentation very well with regard to collision points, collision pairs and predicted injuries compared to sustained injuries. Differences can mainly be linked to differences in vehicle or bicycle geometry, as well as possibly missing documentation of minor injuries (<=AIS2+) in GIDAS in more severe accidents.

Based on the *aim of ATTENTION* and due to time and resource constraints, the alternative approach of

modelling individual bicycles corresponding to the bicycle of each GIDAS case was not considered in this study. The approach of using a mean representative posture and corresponding bicycle for multiple GIDAS cases was further chosen to test how well this setup can reproduce relevant aspects of the vehicle-to-VRU collision. Due to the very good agreement of the data, this approach could also be applicable to other accident cases involving cyclists. The approach taken in this study is very similar to the approach of the Euro NCAP CATS project [35], where a mean bicycle and cyclist based on European data were developed and applied. Nevertheless, it would be an interesting aspect to investigate the effect of different bicycles types, crossbar heights and cyclist positions in future sensitivity studies in comparison with accident data.

For the pelvis, the MPS95 matched the GIDAS information very well, while MPS99 overestimated the AIS2+ injury risk in all cases. For the head, CSDM AIS2+ injury risk best matched the AIS2 TBI of GIDAS, while BrIC overpredicted the injury risk in all cases.

In the selected cases, the most frequent injuries of the injury distribution extracted from comparable GIDAS accident data are covered (A-Fig. 7), except for upper extremity injuries. Based on the good match of HBM simulations with the GIDAS cases, the simulations were also able to reflect the general tendencies shown in A-Fig. 7. To the best knowledge of the authors, there is currently no reliable probabilistic injury criterion available for upper extremity injuries for HBM applications. Therefore, at least based on probabilistic injury assessment, no comparison to GIDAS would have been possible. Only deterministic methods could currently be used for cortical bone fractures in the upper extremities. As no upper extremity injuries were documented in the selected GIDAS, deterministic injury prediction was not analysed for this body region in this study, as described in further detail in the Appendix.

In this study, three collisions were analysed. Based on the small sample size, a determination of trends is not possible. Further, certain factors such as the collision angle might not have been considered in the comparable literature, although they can have an influence on the simulation outcome. Considering this limitation, certain trends observed in this study will be compared with available literature from accident data analysis in the following.

The frontal collision scenarios with crossing cyclists (left to right) presented in this study are also one of the most common accidents in the Swedish Traffic Accident Data Acquisition (STRADA) database, suggesting that the data presented in this study might be equally relevant for other European countries [50].

Based on bicycle accident data, an increase in injury risk can be related to an increase in collision velocity and VRU age [51]. Between the cases 1170987 and 1050918, and between 1170987 and 30090880, an increase in collision velocity led to an increase in injury risk based on GIDAS case data. Further, between the cases 1170987 and 1050918, an increase in age led to an increase in injury risk. Based on GIDAS case data, 1170987 had the lowest overall injury risk, while 1170987 was only slightly smaller than 30090880. In the simulations, the same trend was observed with a higher difference between 1050918 and 30090880 due to the additional leg fracture prediction for 30090880.

Previous studies have shown that leg injuries mainly result from bumper contact, chest injuries from hood or windshield contact and head injuries from windshield, A-pillar, front edge of the roof or ground contact [34]. These trends could also be observed in the simulation data and the respective GIDAS documentation of this study. It should be mentioned that ground impacts were not considered in the numerical part of this study, but only the primary collision with the vehicle. Regarding secondary collisions, for case 1170987 a graze on the forehead due to ground impact and for case 30090880, a TBI I° due to ground impact were documented in GIDAS, matching the previously mentioned findings of other studies. Only head injuries due to front edge of the roof and A-pillar contact were not observed in our study, neither for GIDAS nor for the simulation. This can be directly linked to the selected parameter combination, which would not lead to roof or A-pillar impacts for the types and dimensions of bicycles, vehicles and VRUs involved in the selected GIDAS cases and the corresponding simulations. Therefore, the data from GIDAS and the simulations match the trends very well [34] for the selected

cases for all injury inducing contact pairs. As shown in previous studies, the majority of cyclists sustain minor injuries with a severity of MAIS1 (Maximum Abbreviated Injury Scale) [34]. The majority of injuries reported in GIDAS and predicted via simulations were AIS1 or AIS2 injuries. With regard to AIS itemised injuries, the most commonly injured body regions (AIS1 and AIS2: head, lower and upper extremities) [34] match those of the selected individual GIDAS cases, except for the upper extremity injuries. The latter could not be analysed based on probabilistic injury assessment due to unavailable injury criteria for HBM applications for this body region.

Although the simulation data matches the GIDAS data very well, some uncertainties regarding this comparison remain. On the one hand, the data from the GIDAS accidents might be incomplete or might contain errors to a certain degree. Further, video data is not available in GIDAS, which excludes the possibility of a direct comparison of simulation video data with GIDAS. On the other hand, the model prediction can be the reason for the divergence. This is due to the numerical approximation of the solution by the application of the FE method itself, but also due to necessary simplifications and limitations in the modelling approach, e.g., missing windshield wipers based on the open-source vehicle model, or the averaged bicycle model instead of remodelled versions of each GIDAS bicycle. For the selected GIDAS cases, the crossbar was different from the FE model (A-Fig. 4) and partly also the bicycle type (e.g. mountain bike instead of trekking bike as FE model). Further, as only a passive HBM was used without muscle activation, the stabilising effect of musculature as well as the motion generating aspect are missing in this collision simulation setup. Due to the comparison with accident data, instead of PMHSs, the muscle system would probably play a critical role in the behaviour of the cyclist during a collision and would allow for the additional assessment of muscle strain injury severity [52]. In this study, car-to-cyclist collisions were analysed with an initial car velocity at the time of collision ranging from 30 to 47 km/h. For these collisions the passive THUMS performed quite well. For lower collision velocity collision, it can be assumed that the stabilising effect of the muscular system might play an even more important role. Therefore, further improvement of the simulation results could be obtained by implementing a muscle system in future numerical studies on VRU-vehicle-collisions in comparison to accident data to also achieve biofidelic kinematics and injury predictions in low velocity collision.

Despite these limitations, the models performed very well and led to plausible kinematic behaviour and predicted injuries comparable to the GIDAS accident cases.

V. CONCLUSIONS

In this study, we compared the results of FE collision simulations with single collision cases from the GIDAS accident database. Each model was selected or modelled based on its averaged counterpart in GIDAS. Concluding from the presented data, FE collision simulation using state-of-the-art human body models can be used to replicate accident cases regarding kinematics, collision points, contact pairs and for most of the sustained injuries. Despite minor differences, e.g. in the exact collision point of body parts and car components or an underestimation of the probabilistic tibia fracture prediction in one case, the data from simulation and reality are essentially very comparable. Thus, FE reconstructions of documented vehicle-to-VRU accidents can increase trust in collision simulations, where a validation is not possible due to a lack of PMHS-validation data. Certain limitations of this study are given and could partly be addressed by considering active musculature in FE accident reconstructions of VRU-vehicle collisions in future studies in this field.

VI. ACKNOWLEDGEMENT

This work was supported by the Federal Ministry for Economic Affairs and Climate Action of Germany (Bundesministerium für Wirtschaft und Klimaschutz) through the project *Artificial Intelligence for Real-Time Injury Prediction (ATTENTION)*, Grant Number 19A21027D. Further, the authors would like to thank Christian Kleinbach (Mercedes-Benz AG, Germany) for his contribution in the ATTENTION project, including contributions to the work presented in this study.

VII. REFERENCES

[1] Slootmans, F. (2021) Vias institute, *European Road Safety Observatory. Facts and Figures - Cyclists - 2021*.

[2] Statistisches Bundesamt (destatis). (2021) *Verkehrsunfälle - Kraftrad- und Fahrradunfälle im Straßenverkehr 2020*, Wiesbaden (Germany).

[3] Adminaité-Fodor, D.; Jost, G. (2020) *How safe is walking and cycling in Europe? Pin Flash Report 38*.

[4] Katsuhara, T.; Miyazaki, H.; Kitagawa, Y.; Yasuki, T. (2014) Impact kinematics of cyclist and head injury mechanism in car-to-bicycle collision. *Proceedings of the IRCOBI Conference*, 2014, Berlin (Germany).

[5] Pipkorn, B. (2021) State-of-the-Art Human Body Modelling (HBM) Analysis for Cyclist Airbags, 2021, Virtual conference.

[6] Leo, C.; Gruber, M.; Feist, F.; Sinz, W.; Roth, F.; Klug, C. (2020) The Effect of Autonomous Emergency Braking Systems on Head Impact Conditions for Pedestrian and Cyclists in Passenger Car Collisions. *Proceedings of the IRCOBI Conference*, 2020, Munich (Germany).

[7] Klug, C.; Feist, F.; Wimmer, P. (2018) Simulation of a Selected Real World Car to Bicyclist Accident using a Detailed Human Body Model. *Proceedings of the IRCOBI Conference*, 2018, Athen (Greece).

[8] N. Bourdet; C. Deck; T. Serre; C. Perrin; M. Llari; R. Willinger. (2014) In-depth real-world bicycle accident reconstructions. International Journal of Crashworthiness, **19**(3): 222–232.

[9] Shigeta, K.; Kitagawa, Y.; Yasuki, T. (2009) Development of Next Generation Human FE Model capable of Organ Injury Prediction. *Proceedings of the 21st Annual Enhanced Safety of Vehicles*, 2009, Stuttgart (Germany).

[10] Untaroiu, C. D.; Pak, W.; Meng, Y.; Schap, J.; Koya, B.; Gayzik, S. (2017) A Finite Element Model of a Midsize Male for Simulating Pedestrian Accidents. Journal of Biomechanical Engineering, **140**(1).

[11] John, J.; Klug, C.; Kranjec, M.; Svenning, E.; Iraeus, J. (2022) Hello, world! VIVA+: A human body model lineup to evaluate sex-differences in crash protection. Frontiers in bioengineering and biotechnology, **10**(918904).

[12] Toyota Motor Corporation, Toyota Central R&D Labs., Inc. (2021) *Documentation Total Human Model for Safety (THUMS) AM50 Pedestrian Model Version 4.02*.

[13] Wu, T.; Kim, T. et al. (2017) Evaluation of biofidelity of THUMS pedestrian model under a whole-body impact conditions with a generic sedan buck. Traffic injury prevention, **18**(sup1): S148-S154.

[14] Forman, J. L.; Joodaki, H. et al. (2015) Whole-body Response for Pedestrian Impact with a Generic Sedan Buck. Stapp Car Crash Journal, **59**: 401–444.

[15] Forman, J. L.; Joodaki, H. et al. (2015) Biofidelity Corridors for Whole-Body Pedestrian Impact with a Generic Buck. *Proceedings of the IRCOBI Conference*, 2015, Lyon (France).

[16] Matt, P.; Jenerowicz, M.; Schweiger, T.; Heisch, F.; Lienhard, J.; Boljen, M. (2022) Investigation of e-scooter drivers colliding with kerbs–a parametric numerical study. *Proceedings of the IRCOBI Conference*, 2022, Porto (Portugal).

[17] Trube, N.; Matt, P.; Boljen, M. (2020) A Numerical Study on Pedestrian and Wheelchair User Safety in VRU-Vehicle Collisions. *Proceedings of the IRCOBI Conference*, 2020, Munich (Germany).

[18] Lich, T.; Moennich, J.; and Schmidt, D.; Voss, M. (2022) Preparation of an AI based real-time injury risk index estimation by deriving road user behavior from video-documented crashes. *15th International Symposium and Exhibition on Sophisticated Car Safety System (airbag2022)*, 2022, Mannheim (Germany).

[19] Lich, T.; Mönnich, J.; Voss, M.; Lerge, P.; Nölle, L. V.; Schmitt, S. (2023) Applying AI Methods On Video Documented Car-VRU Front Crashes to Determine Generalized Vulnerable Road User Behaviors. *Proceedings of the 27th International Technical Conference on the Enhanced Safety of Vehicles (ESV)*, 2023, Yokohama (Japan).

[20] Klug, C.; Ellway, J. (2021) *Pedestrian Human Model Certification. Technical Bulletin TB024 Version 3.0.1*.

[21] "German in-depth accident study (GIDAS) – Data 2001 – 2022", Available: www.gidas.org. [May 2023].

[22] Liers, H. (2018) Traffic accident research in Germany and the German in-depth accident study (GIDAS). *Society of Indian Automotive Manufactures (SIAM) Conference*, 2018.

[23] Ballal, N.; Soot, T.; Dlugosch, M.; Trube, N.; Fressmann, D. (2023) A method for efficient generation and optimization of simulation-based training data for data-driven injury prediction in vru-vehicle accident scenarios. *Proceedings of the 27th International Technical Conference on the Enhanced Safety of Vehicles (ESV)*, 2023, Yokohama (Japan).

[24] Center for Collision Safety and Analysis at the George Mason University (GMU), Federal Highway Administration (FHWA). "Toyota Camry Detailed Finite Element Model", Available: https://www.ccsa.gmu.edu/models/2012-toyota-camry. [May 2023].

[25] Peng, Y.; Yang, J.; Deck, C.; Willinger, R. (2013) Finite Element Modeling of Crash Test Behavior for Windshield Laminated Glass. International Journal of Impact Engineering, **57**: 27–35.

[26] Kulkarni, N.; Deshpande, S.; Mahajan, R. (2019) Development of Pedestrian Headform Finite Element Model using LS-DYNA and its Validation as per AIS 100/GTR9. *Proceedings of the 12th European LS-Dyna Conference*, 2019, Koblenz (Germany).

[27] J. Prasongngen, I. Putra, S. Koetniyom and J. Carmai. (2013) Improvements of Windshield Laminated Glass Model for Finite Element Simulation of Head-to-Windhsield Impacts. *IOP Conference*, 2013, Phuket (Thailand).

[28] Osnes, K.; Kreissl, S.; D'Haen, J.; Borvik, T. (2021) Modelling of Fracture Initiation and Post-Fracture Behaviour of Head Impact on Car Windshields. *Proceedings of the 13th European LS-Dyna Conference*, 2021, Ulm (Germany).

[29] Jaware, A.; Chandratre, S.; Perez, M.; Narule, J. (2019) An Advanced Methodology for Windscreen Modeling in LS Dyna. International Journal of Mechanical Engineering and Technology (IJMET), **10**(12).

[30] Alter, C.; Kolling, S.; Schneider, J. (2018) A new failure criterion for laminated safety glass. *Proceedings of the 11th European LS-Dyna Conference*, 2018, Salzburg (Austria).

[31] Chen, S.; Zang, M.; Wang, D.; Zheng, Z.; Zhao, C. (2016) Finite element modelling of impact damage in polyvinyl butyral laminated glass. Composite Structures, **138**: p. 1–11.

[32] National Highway Traffic Safety Administration (NHTSA). "2011 Honda Accord Detailed Finite Element Model", Available: https://www.nhtsa.gov/crash-simulation-vehicle-models. [May 2023].

[33] Maurath Sommer, C.; Burger, M.; Day, E. (2018) Livermore Software Technology Corp. (LSTC)., *LSTC Adult Pedestrian Headform User's Guide. Version: LSTC.PEDESTRIAN_HEADFORM_ADULT.180601_V1.06.BETA.*

[34] Hamacher, M.; Kühn, M.; Hummel, T. (2016) *Analyse der Radfahrer-Pkw-Kollision*, 65. *Gesamtverband der Deutschen Versicherungswirtschaft e.V. Unfallforschung der Versicherer*, Berlin (Germany).

[35] Camp, O. O. den; van Montfort, S.; Uittenbogaard, J. (2016) *CATS Deliverable 6.1: CATS Final project summary report. TNO report*.

[36] Takhounts, E. G.; Craig, M. J.; Moorhouse, K.; McFadden, J.; Hasija, V. (2013) Development of brain injury criteria (BrIC). Stapp Car Crash Journal, **57**: 243–266.

[37] Takhounts, E. G.; Eppinger, R. H.; Campbell, J. Q.; Tannous, R. E.; Power, E. D.; Shook, L. S. (2003) On the Development of the SIMon Finite Element Head Model. Stapp Car Crash Journal, **47**: 107–133.

[38] Takhounts, E. G.; Ridella, S. A. et al. (2008) Investigation of traumatic brain injuries using the next generation of simulated injury monitor (SIMon) finite element head model. Stapp Car Crash Journal, **52**: 1–31.

[39] Forman, J. L.; Kent, R. W.; Mroz, K.; Pipkorn, B.; Bostrom, O.; Segui-Gomez, M. (2012) Predicting rib fracture risk with whole-body finite element models: development and preliminary evaluation of a probabilistic analytical framework. *Proceedings of the 56th annual AAAM Scientific Conference*, 2012, Seattle, Washington (USA).

[40] Iraeus, J.; Lindquist, M. (2021) Analysis of minimum pulse shape information needed for accurate chest

injury prediction in real life frontal crashes. International Journal of Crashworthiness, **26**(6): 684–691.

[41] Mayer, C.; Iraeus, J. et al. (2022) *Criteria and risk functions for prediction of injury risks in new sitting positions and new crash scenarios. OSCCAR Deliverable D3.3*.

[42] Gunji, Y.; Okamoto, M.; Takahashi, Y. (2012) Examination of human body mass influence on pedestrian pelvis injury prediction using a human FE model. *Proceedings of the IRCOBI Conference*, 2012, Dublin (Ireland).

[43] Peres, J.; Auer, S.; Praxl, N. (2016) Development and comparison of different injury risk functions predicting pelvic fractures in side impact for a Human Body Model. *Proceedings of the IRCOBI Conference*, 2016, Malaga (Spain).

[44] Kerrigan, J. R.; Drinkwater, D. C.; Kam, C. Y.; Murphy, D. B.; Ivarsson. (2004) Tolerance of the human leg and thigh in dynamic latero-medial bending. International Journal of Crashworthiness, **9**(6): 607–623.

[45] Kuppa, S.; Wang, J.; Haffner, M.; Eppinger, R. (2001) Lower extremity injuries and associated injury criteria. SAE Technical Paper,

[46] Association for the Advancement of Automotive Medicine. (2016) Association for the Advancement of Automotive Medicine, *The Abbreviated Injury Scale - 2015 revision*, Chicago, Illinous (USA).

[47] Snedeker, J. G.; Muser, M. H.; Walz, F. H. (2003) Assessment of pelvis and upper leg injury risk in car-pedestrian collisions: comparison of accident statistics, impactor tests and a human body finite element model. Stapp Car Crash Journal, **47**: 437–457.

[48] Golman, A. J.; Danelson, K. A.; Miller, L. E.; Stitzel, J. D. (2014) Injury prediction in a side impact crash using human body model simulation. Accident Analysis & Prevention, **64**: 1–8.

[49] Yasuki, Tsuoyoshi, and Yasuo Yamamae. (2010) Validation of kinematics and lower extremity injuries estimated by total human model for safety in SUV to pedestrian impact test. Journal of Biomechanical Science and Engineering, **5**(4): 340–356.

[50] Fredriksson, R.; Fredriksson, K.; Strandroth, J. (2014) Pre-crash motion and conditions of bicyclist-to-car crashes in Sweden. *Proceedings of the International Cycling Safety Conference*, 2014, Göteborg (Sweden).

[51] Moennich, J.; Lich, T.; Georgi, Andreas, Reiter, Nora. (2015) *Did a higher distribution of pedelecs results in more severe accidents in Germany?*

[52] Nölle, L. V.; Mishra, A.; Martynenko, O. V.; Schmitt, S. (2022) Evaluation of muscle strain injury severity in active human body models. Journal of the mechanical behavior of biomedical materials, **135**: 105463.

VIII. APPENDIX

The whole-body kinematics from simulation is shown over time for each case in A-Fig. 1 to A-Fig. 3.

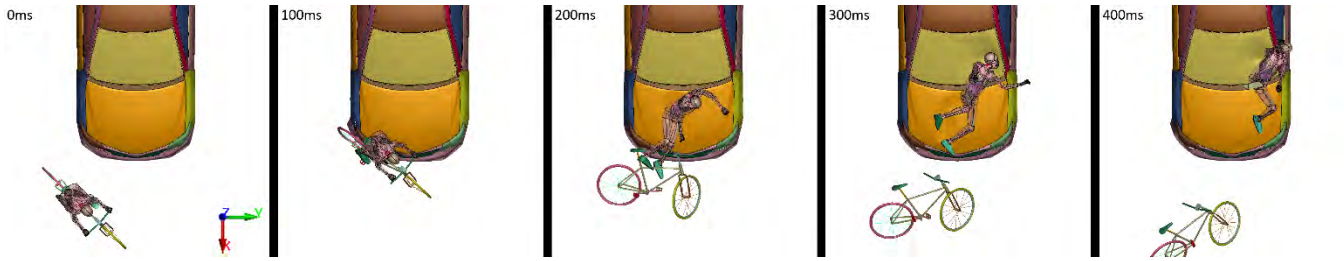

A-Fig. 1. Whole-body kinematics over time from simulation data for case 1050918.

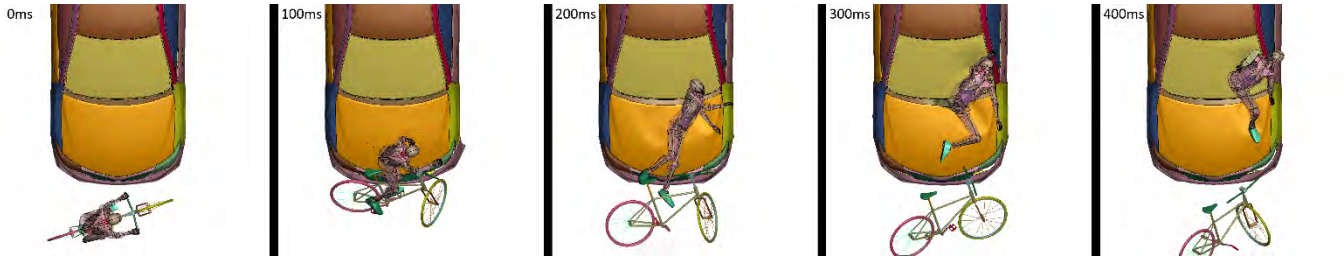

A-Fig. 2. Whole-body kinematics over time from simulation data for case 1170986.

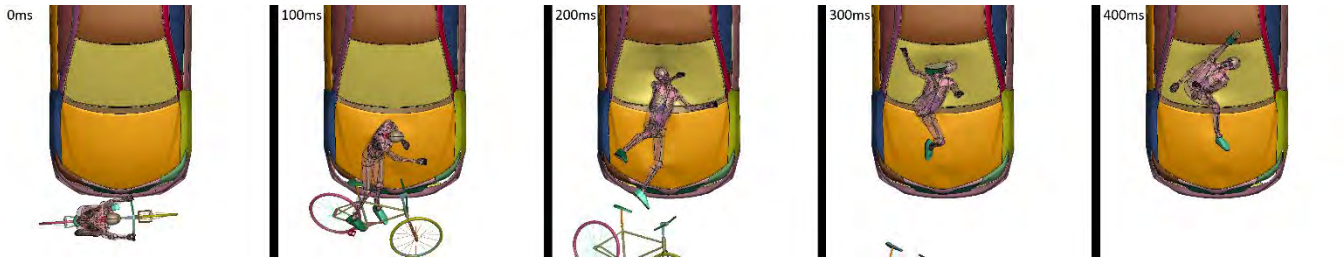

A-Fig. 3. Whole-body kinematics over time from simulation data for case 30090880.

In A-Fig. 4 a comparison between the bicycle FE model and the three bicycles of the GIDAS cases is shown.

FE model	1050918	1170986	30090880
			

A-Fig. 4. Comparison of the bicycle FE model and the bicycles of each GIDAS case.

In A-Fig. 5, the comparison of individual collision points of specific body parts with vehicle components between GIDAS and the FE simulation is shown.

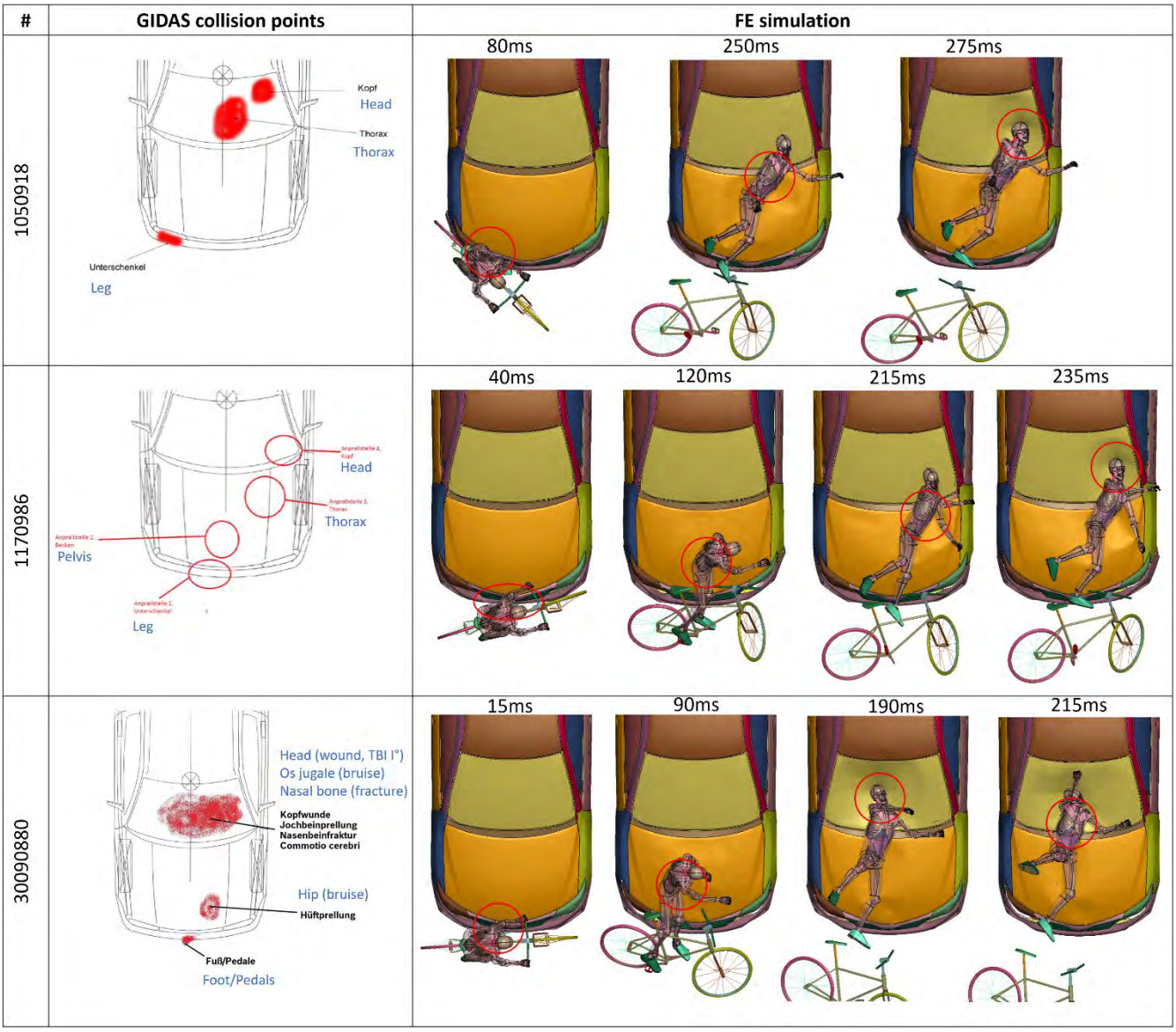

A-Fig. 5. Collision points of the cyclist and the vehicle in accident data and in the collision simulations regarding the documented body regions. English translations were added in blue based on the original image file from GIDAS.

In A-Fig. 6, the documented injury-inducing GIDAS contact pairs and the corresponding resultant force data from simulation are compared for each accident case. For each individual injury, a vehicle component was assigned as the primary contact partner in the GIDAS documentation.

#	GIDAS contact pairs and resultant contact forces
1050918	1) Tibia and Fibula fracture (left) → Bumper of opposing vehicle 2) TBI I° → Windshield of opposing vehicle
1170986	1) Bruise leg (left) → Bumper of opposing vehicle 2) Graze knee (left) → Hood of opposing vehicle 3) Graze D1 (left), inner ankle (left), leg (right) → Own bicycle, footpegs, pedals 4) Graze forehead (left), TBI I° → Windshield of opposing vehicle
30090880	1) Bruise hip (left) → Hood of opposing vehicle 2) Fractured ribs (L8, L9) → Hood of opposing vehicle 3) TBI I°, Nasal bone fracture, Bruise os jugale (right), Parietal wound head (left) → Windshield of opposing vehicle

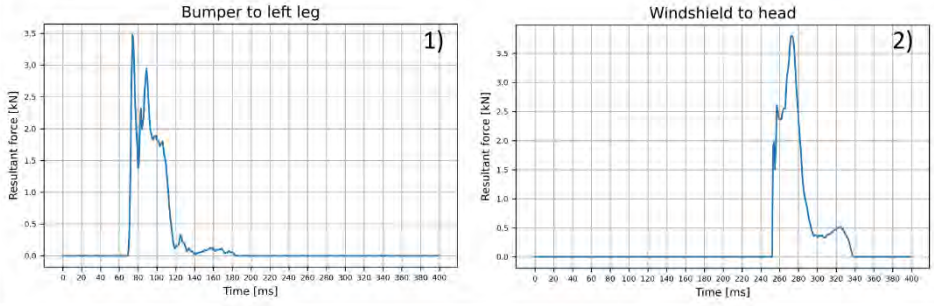

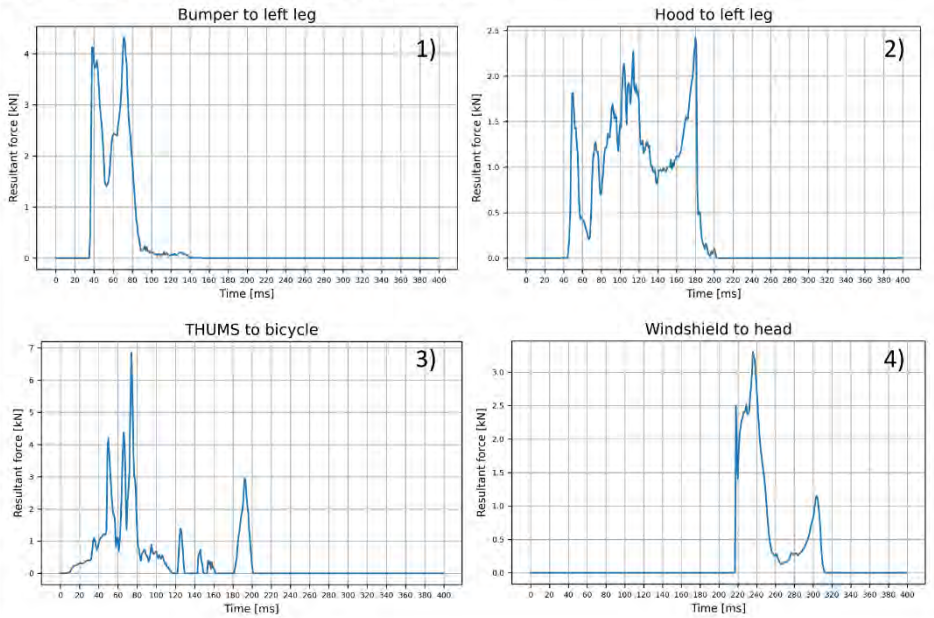

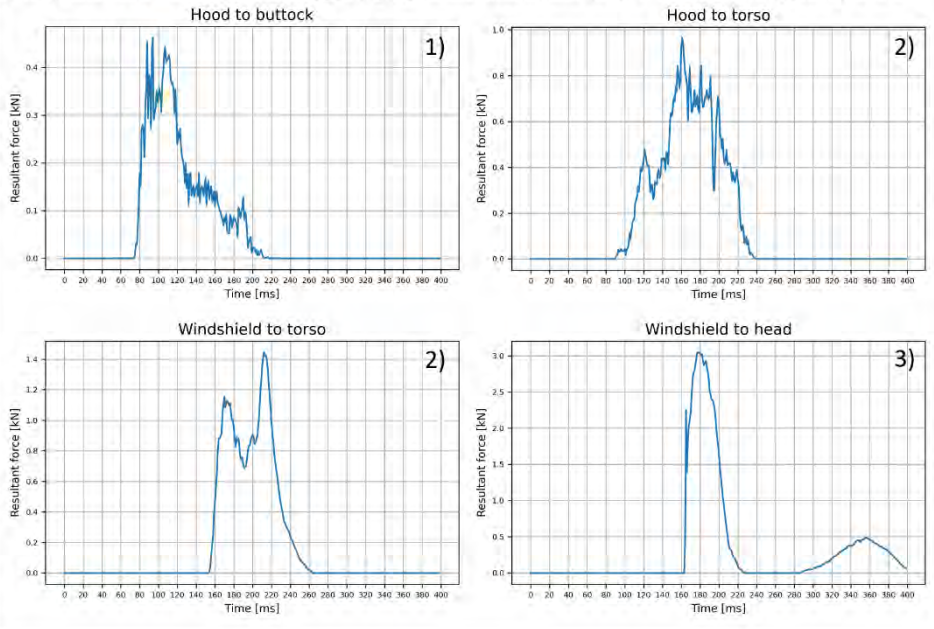

A-Fig. 6. Contact pairs in GIDAS compared with resultant contact forces between THUMS body parts and vehicle components.

Data on injury distributions from the GIDAS database are shown in A-Fig. 7, which was created based on accident data that fulfilled certain criteria, such as the type of collision (A), as well as the vehicle dimensions and body sizes in comparison to the respective FE models of this study (B).

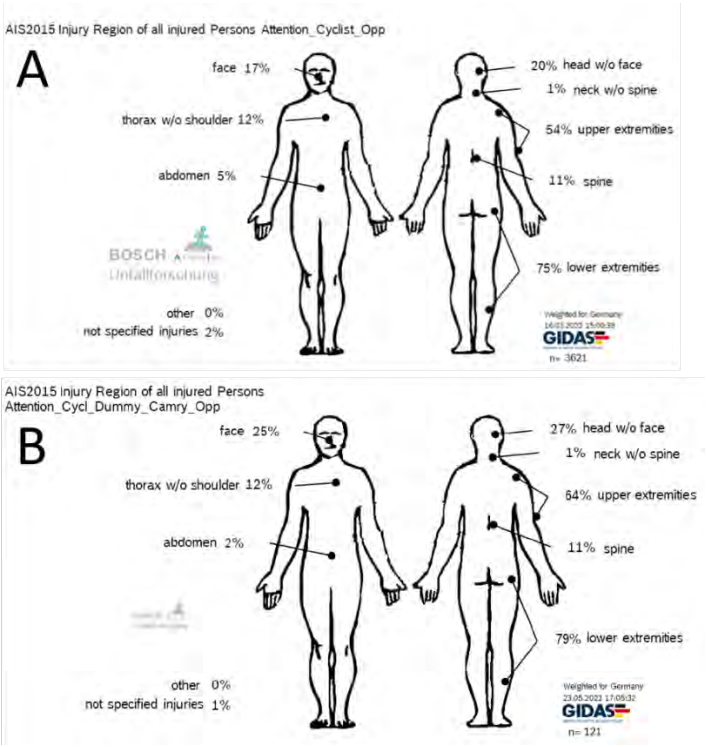

A-Fig. 7. Injury distribution of two GIDAS datasets. A) GIDAS database filtered mainly by frontal collisions; B) Further filtering based on *A* regarding cases where the vehicle sizes match those of the Toyota Camry FE model and where the body sizes match those of the THUMS.

In Table A-I to Table A-III, details regarding sustained injuries (GIDAS) and predicted injuries (HBM) are presented. Regarding deterministic injury prediction, the following bones were considered if multiple bones were relevant for a body region. For the ribs, all left and right ribs were considered with one maximum MPS value per rib. Based on this data, the maximum values as well as the 2nd and 3rd highest values of all ribs were calculated. For the lumbar spine, the L1 to L5 were considered. For the pelvis, the sacrum and all hipbones were considered. For the ankle, the talus and calcaneus were considered. For the foot, all cortical bones in the foot (except talus and calcaneus) were considered. For the other bones, individual cortical bone data could be used, e.g., right femur. Data on cortical bones are listed, for which an injury was documented in at least one of the three GIDAS cases. Grazes and bruises are generally documented as AIS1 injuries in GIDAS. For the evaluation of the probabilistic femur and tibia fracture criteria, the resultant moment ($M_{Resultant}$) [44] and the Revised Tibia Index (RTI) [45] were applied.

TABLE A-I

SUSTAINED AND PREDICTED INJURIES FOR GIDAS CASE 1050918

GIDAS		Probabilistic prediction			Deterministic prediction		
Region	Injury	Injury criterion	Injury value	Injury risk	Region	Max MPS	Threshold
Head	Traumatic brain injury I° (TBS, AIS2)	CSDM	0.35	AIS1+=100 %, AIS2+=72.9 % AIS3+=41.7 % AIS4+=31.2 % AIS5+=29.5 %	-	-	-
	Head laceration (AIS1)	BrIC	1.29	AIS1+=100 %, AIS2+=99.9 % AIS3+=88.2 % AIS4+=70.3 % AIS5+=66.2 %			
Thorax	-	Forman		AIS1+=10.3 % AIS2+=0.5 % AIS3+=0.0 %	Ribs	Max=1.27 % Max_{2nd}=1.12 % Max_{3rd}=1.06 %	1.5 %
Lumbar spine	-	-	-	-		Max=0.75 %	1.5 %
Pelvis	-	Quartile value of MPS distribution	Q95=0.19 % Q99=1.35 %	AIS2+_45=1.5 % AIS2+_65=4.4 % AIS2+_45=67.6 % AIS2+_65=80.2 %		Max=0.42 %	1.0 %
		Deflection	0.63 mm	AIS2+=0.47 %			
R Thigh	-	$M_{Resultant}$ Mid-femur Mid-thigh Dist-femur Dist-thigh	 135.3 Nm 122.5 Nm 150.6 Nm 145.1 Nm	 AIS3+=0.1 % AIS3+=0.02 % AIS3+=0.6 % AIS3+=0.19 %		3.59 %	1.5 %
L Thigh	-	$M_{Resultant}$ Mid-femur Mid-thigh Dist-femur Dist-thigh	 78.8 Nm 91.1 Nm 72.9 Nm 84.8 Nm	 AIS3+=0.0 % AIS3+=0.0 % AIS3+=0.01 % AIS3+=0.01 %		0.48 %	1.5 %
R Knee	-	-	-	-		2.7 %	1.5 %
L Knee	-	-	-	-		0.28 %	1.5 %
R Leg	-	RTI Proximal Distal $M_{Resultant}$ Mid-Leg	 0.45 0.21 115.9 Nm	 AIS2+=1.31 % AIS2+=0.06 % AIS2+=0.25 %		Tib:1.15 % Fib:0.98 %	1.5 %
L Leg	Tibia & fibula Fracture (AIS2)	RTI Proximal Distal $M_{Resultant}$ Mid-Leg	 0.51 0.76 159.85 Nm	 AIS2+=2.09 % AIS2+=10.53 % AIS2+=1.53 %		Tib:2.22 % Fib:1.28 %	1.5 %
R Ankle	-	-	-	-		Max=0.72 %	1.5 %
L Ankle	-	-	-	-		Max=0.81 %	1.5 %
R Foot	-	-	-	-		Max=0.53 %	1.5 %
L Foot	-	-	-	-		Max=0.62 %	1.5 %

TABLE A-II

SUSTAINED AND PREDICTED INJURIES FOR GIDAS CASE 1170986

GIDAS		Probabilistic prediction			Deterministic prediction		
Region	Injury	Injury criterion	Injury value	Injury risk	Region	Max MPS	Threshold
Head	TBS I° (AIS2) Graze forehead (AIS1)	CSDM	0.28	AIS1+=100 %, AIS2+=57.8 % AIS3+=30.0 % AIS4+=21.9 % AIS5+=20.6 %	-	-	-
		BrIC	1.17	AIS1+=100 %, AIS2+=99.9 % AIS3+=79.9 % AIS4+=59.8 % AIS5+=55.8 %			
Thorax	-	Forman		AIS1+=10.3 % AIS2+=0.4 % AIS3+=0.0 %	Ribs	Max=1.37 % Max_{2nd}=1.03 % Max_{3rd}=0.80 %	1.5 %
Lumbar spine	2 minimally dislocated bony fragments of the anterior edge of the L5 vertebra (AIS2)			-		Max=0.49 %	1.5 %
Pelvis	-	Quartile value of MPS distribution	Q95=0.26 % Q99=1.49 %	AIS2+_45=7.0 % AIS2+_65=15.6 % AIS2+_45=75.0 % AIS2+_65=85.7 %		Max=0.40 %	1.0 %
		Deflection	0.79 mm	AIS2+=0.97			
R Thigh	-	$M_{Resultant}$				5.84 %	1.5 %
		Mid-femur	106.2 Nm	AIS3+=0.02 %			
		Mid-thigh	99.6 Nm	AIS3+=0.01 %			
		Dist-femur	97.1 Nm	AIS3+=0.04 %			
		Dist-thigh	91.1 Nm	AIS3+=0.01 %			
L Thigh	-	$M_{Resultant}$				0.61 %	1.5 %
		Mid-femur	153.6 Nm	AIS3+=0.22 %			
		Mid-thigh	150.3 Nm	AIS3+=0.08 %			
		Dist-femur	148.8 Nm	AIS3+=0.56 %			
		Dist-thigh	143.1 Nm	AIS3+=0.18 %			
R Knee	Graze	-	-	-		4.08 %	1.5 %
L Knee	Graze	-	-	-		0.71 %	1.5 %
R Leg	Graze	RTI				Tib:1.24 %	1.5 %
		Proximal	0.51	AIS2+=2.12 %		Fib:0.74 %	
		Distal	0.27	AIS2+=0.17 %			
		$M_{Resultant}$					
		Mid-Leg	82.1 Nm	AIS2+=0.03 %			
L Leg	Bruise	RTI				Tib:3.54 %	1.5 %
		Proximal	0.44	AIS2+=1.15 %		Fib:2.37 %	
		Distal	0.74	AIS2+=9.38 %			
		$M_{Resultant}$					
		Mid-Leg	191.25 Nm	AIS2+=4.18 %			
R Ankle	-	-	-	-		Max=1.10 %	1.5 %
L Ankle	Graze	-	-	-		Max=0.61 %	1.5 %
R Foot	-	-	-	-		Max=0.63 %	1.5 %
L Foot	Graze	-	-	-		Max=0.60 %	1.5 %

TABLE A-III

SUSTAINED AND PREDICTED INJURIES FOR GIDAS CASE 30090880

GIDAS		Probabilistic prediction			Deterministic prediction		
Region	Injury	Injury criterion	Injury value	Injury risk	Region	Max MPS	Threshold
Head	TBS I° (AIS2) Bruise (Os jugale, AIS1) Parietal wound head, L (AIS1) Nasal bone fracture (AIS1)	CSDM	0.39	AIS1+=100 %, AIS2+=80.2 % AIS3+=48.8 % AIS4+=37.2 % AIS5+=35.1 %	-	-	-
		BrIC	1.34	AIS1+=100 %, AIS2+=99.9 % AIS3+=90.7 % AIS4+=74.1 % AIS5+=70.1 %			
Thorax	Fracture L8, L9 (AIS2)	Forman		AIS1+=29.4 % AIS2+=2.5 % AIS3+=0.1 %	Ribs	Max=1.83 % Max_{2nd}=1.04 % Max_{3rd}=0.85 %	1.5 %
Lumbar spine	-	-	-	-		Max=1.33 %	1.5 %
Pelvis	Bruise (AIS1)	Quartile value of MPS distribution	Q95=0.36 %	AIS2+_45=22.0 % AIS2+_65=37.9 %		Max=1.20 %	1.0 %
			Q99=1.9 %	AIS2+_45=88.5 % AIS2+_65=94.4 %			
		Deflection	0.79 mm	AIS2+=0.99 %			
R Thigh	-	$M_{Resultant}$				6.51 %	1.5 %
		Mid-femur	182.2 Nm	AIS3+=0.63 %			
		Mid-thigh	175.1 Nm	AIS3+=0.20 %			
		Dist-femur	171.3 Nm	AIS3+=1.86 %			
		Dist-thigh	179.4 Nm	AIS3+=0.73 %			
L Thigh	-	$M_{Resultant}$				0.75 %	1.5 %
		Mid-femur	171.3 Nm	AIS3+=0.43 %			
		Mid-thigh	189.4 Nm	AIS3+=0.33 %			
		Dist-femur	159.6 Nm	AIS3+=0.87 %			
		Dist-thigh	170.66 Nm	AIS3+=0.53 %			
R Knee	-	-	-	-		3.64 %	1.5 %
L Knee	-	-	-	-		0.5 %	1.5 %
R Leg	-	RTI				Tib:1.10 %	1.5 %
		Proximal	0.53	AIS2+=2.58 %		Fib:1.13 %	
		Distal	0.51	AIS2+=2.16 %			
		$M_{Resultant}$					
		Mid-Leg	136.4 Nm	AIS2+=0.62 %			
L Leg		RTI				Tib:5.38 %	1.5 %
		Proximal	0.43	AIS2+=1.12 %		Fib:2.96 %	
		Distal	1.08	AIS2+=36.23 %			
		$M_{Resultant}$					
		Mid-Leg	228.1 Nm	AIS2+=10.99 %			
R Ankle	-	-	-	-		Max=1.65 %	1.5 %
L Ankle	-	-	-	-		Max=1.66 %	1.5 %
R Foot	-	-	-	-		Max=0.58 %	1.5 %
L Foot	-	-	-	-		Max=0.57 %	1.5 %

Additional data on the validation of the windshield model is provided in A-Fig. 8.

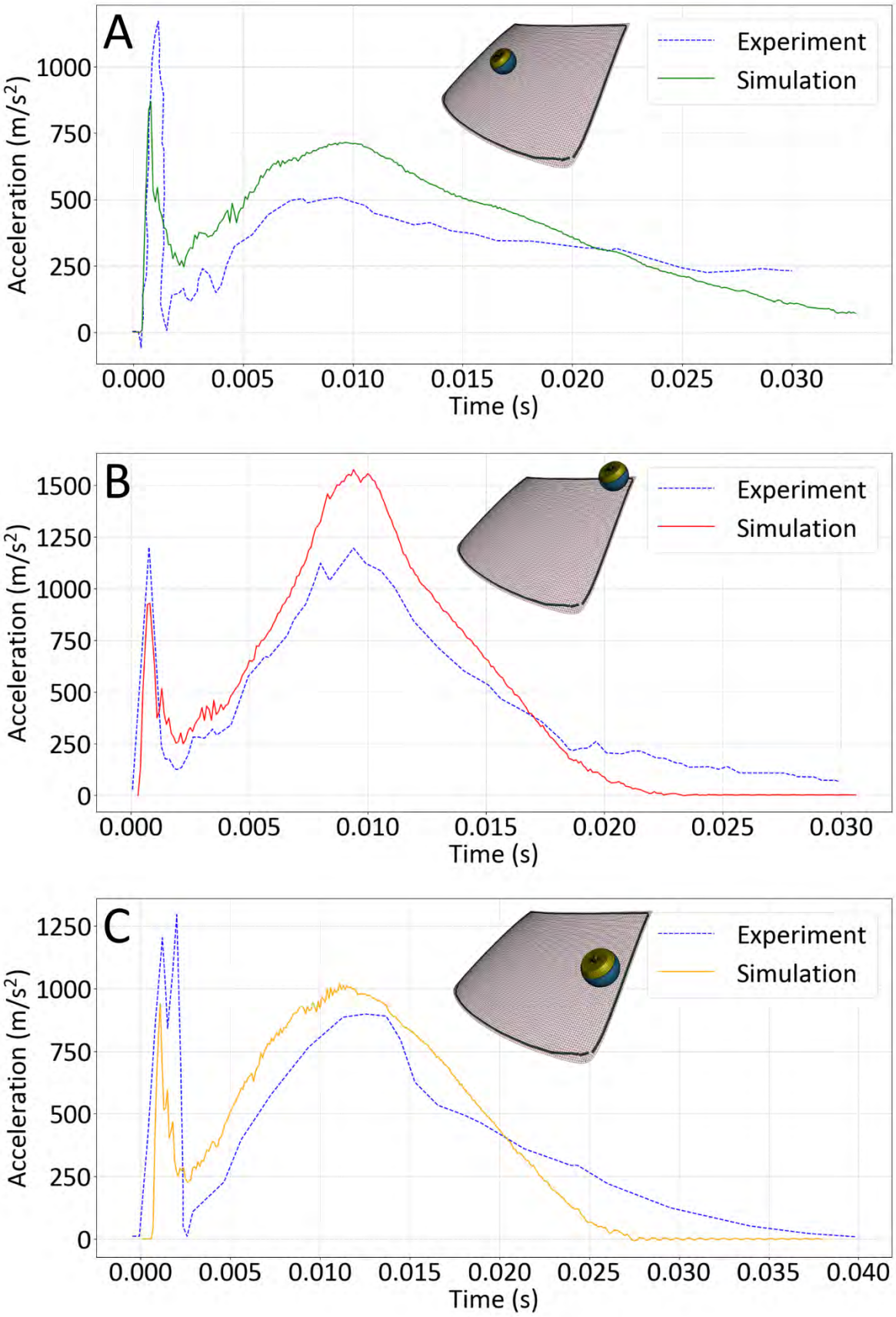

A-Fig. 8. Comparison of the three different positions (A) centre [25, 27], B) corner [28] and C) side [25, 27]) of a standard EEVC headform impactor [33] impacting the windshield. In reference [28] the acceleration values are given as products of a scalar for the corner load case.